ARTICLES

nature
structural biology



# The crystal structure of the proprotein processing proteinase furin explains its stringent specificity

Stefan Henrich[1], Angus Cameron[2,5], Gleb P Bourenkov[3], Reiner Kiefersauer[1,4], Robert Huber[1], Iris Lindberg[2], Wolfram Bode[1] & Manuel E Than[1]

**In eukaryotes, many essential secreted proteins and peptide hormones are excised from larger precursors by members of a class of calcium-dependent endoproteinases, the prohormone-proprotein convertases (PCs). Furin, the best-characterized member of the mammalian PC family, has essential functions in embryogenesis and homeostasis but is also implicated in various pathologies such as tumor metastasis, neurodegeneration and various bacterial and viral diseases caused by such pathogens as anthrax and pathogenic Ebola virus strains. Furin cleaves protein precursors with narrow specificity following basic Arg-Xaa-Lys/Arg-Arg-like motifs. The 2.6 Å crystal structure of the decanoyl-Arg-Val-Lys-Arg-chloromethylketone (dec-RVKR-cmk)–inhibited mouse furin ectodomain, the first PC structure, reveals an eight-stranded jelly-roll P domain associated with the catalytic domain. Contoured surface loops shape the active site by cleft, thus explaining furin's stringent requirement for arginine at P1 and P4, and lysine at P2 sites by highly charge-complementary pockets. The structure also explains furin's preference for basic residues at P3, P5 and P6 sites. This structure will aid in the rational design of antiviral and antibacterial drugs.**

Many secreted proteins, hormones, enzymes and neuropeptides are initially synthesized as inactive precursors (or proproteins) and activated only through a controlled proteolytic cleavage by prohormone-proprotein convertases (PCs)[1–5]. Seven members of the PC family (furin, PC1/PC3, PC2, PACE4, PC4, PC5/PC6 and PC7/PC8/LPC/SPC7) have been identified in humans and other mammals and found to be homologous to the yeast endoproteinase Kex2/kexin[6,7]. Furin (also called SPC1/PACE; EC 3.4.21.75, MEROPS clan SB, family S8), so far the best-characterized member, is a type I transmembrane glycoprotein of ~96 kDa that is translated as a 794-residue preproenzyme (793 residues in mouse; **Fig. 1**) and expressed in all tissues and cells that have been examined. The N-terminal 83-residue propeptide (residues Gln25–Arg107), which has a critical role in folding, is autocatalytically excised from the inactive zymogen but remains associated with the mature domain, functioning as a powerful auto-inhibitor. During migration to the more acidic trans-Golgi network (TGN), the prosegment dissociates after a second internal autocatalytic cleavage between Arg75 and Ser76, releasing catalytically active furin[8,9], which consists of a catalytic domain, a P/homoB domain essential for activity and a C-terminal tail containing a transmembrane helix. Furin cycles between the TGN, the cell surface and the endosomal compartments[4,9], where it processes a diverse collection of membrane-bound and soluble precursors of growth factors, receptors, plasma proteins, Alzheimer-related secretases and cancer-associated extracellular matrix proteinases. Furin fulfills essential functions in embryogenesis[10] and homeostasis, but it is also required for the activation of many bacterial toxin precursors (including *Pseudomonas aeruginosa*, diphtheria and anthrax toxins[11]) as well as for the processing of virus envelope glycoproteins (for example, those from pathogenic Ebola strains[12], HIV-1 gp160 (ref. 13) or the avian influenza virus hemagglutinin[1,4,5]). In addition to membrane-bound forms, naturally truncated 'shed' furin species have also been identified and shown to be functionally active as endoproteinases *in vivo* and *in vitro*[9,11]. Despite the importance of furin and the other PCs for essential physiological processes as well as involvement in many severe diseases, no crystal structure of any PC member has yet been obtained. The solution structure of the PC1/PC3 prodomain has been determined by NMR spectroscopy[14], and models of the catalytic[15] and of the P domain[16] have been made on the basis of bacterial subtilisins and secondary structure predictions. Here, we show for the first time the crystal structure of furin comprising the catalytic and P domains, thus explaining the potential function of the P domain, the stringent substrate specificity of this enzyme and additional functional aspects. This structure should be of importance for the development of specific inhibitors of furin.

## RESULTS

### Overall structure

We have crystallized soluble mouse furin (Asp108 to about Pro582), comprising the catalytic and the P domains, in hexagonal and in

[1]Max-Planck-Institut für Biochemie, Abt. Strukturforschung, Am Klopferspitz 18A, 82152 Martinsried, Germany. [2]Louisiana State University Health Sciences Center, Department of Biochemistry & Molecular Biology, 1901 Perdido Street, New Orleans, Louisiana 70112, USA. [3]Max-Planck-Arbeitsgruppen für Strukturelle Molekularbiologie (MPG-ASMB), Gruppe Proteindynamik, DESY, Notkestrasse 85, 22603 Hamburg, Germany. [4]Proteros Biostructures GmbH, Am Klopferspitz 19, 82152 Martinsried, Germany. [5]Present address: University of Bristol, Department of Biochemistry, University Walk, Bristol, BS8 1TD, United Kingdom. Correspondence should be addressed to W.B. (bode@biochem.mpg.de) or M.E.T. (than@biochem.mpg.de).

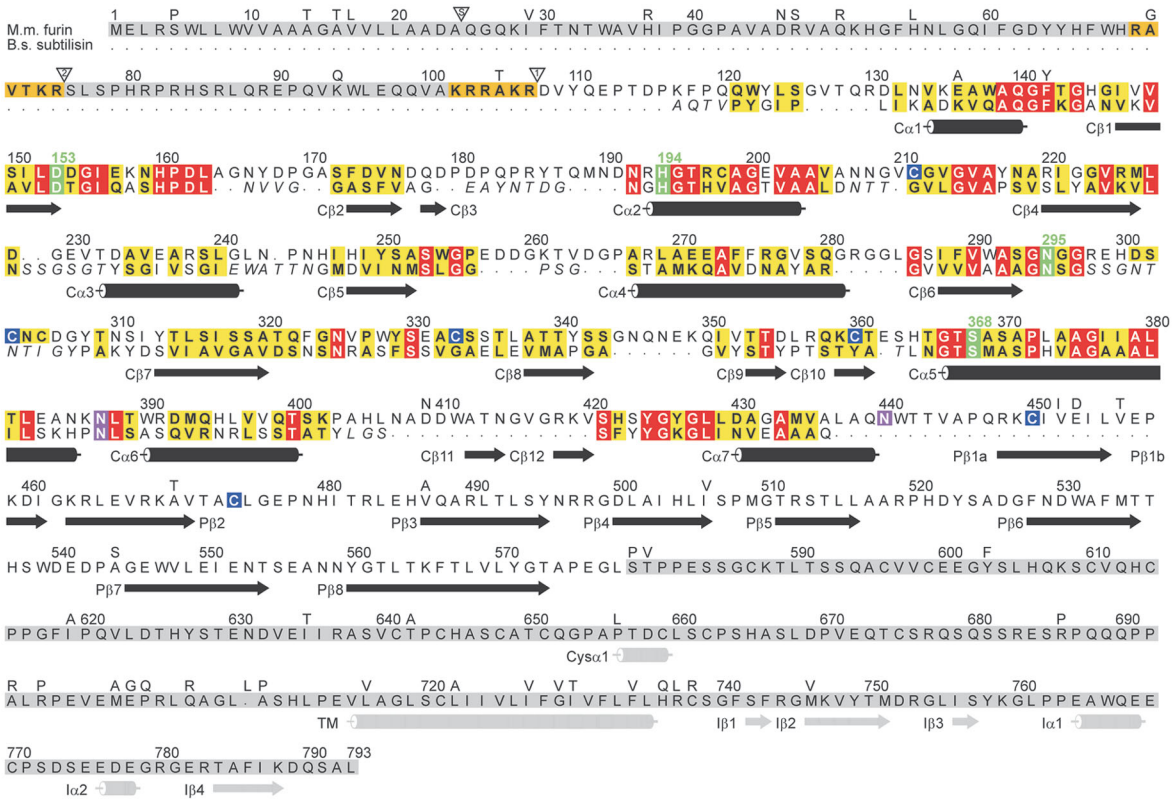


**Figure 1** Primary structure of mouse furin. Structure-based amino acid sequence alignment of mouse furin (M.m. furin) and subtilisin Carlsberg (B.s. subtilisin). For subtilisin, all topologically nonequivalent residues are italic. Identical and similar residues are red and yellow, respectively; cysteine residues are blue, the active site residues green and the two glycosylated asparagine residues pink. The nonprime residues of the primary and secondary activation sites (numbered arrowheads) are shown with an orange background, and the signal-peptide cleavage site is indicated by the S-labeled arrowhead. The numbering used is for intact translated mouse furin, with the few substitutions in the human enzyme indicated above the mouse sequence. Below the sequence, β-strands and helices of furin are indicated by arrows and cylinders, shown in black as experimentally derived for the catalytic and the P domain, and in light gray as predicted for the more C-terminal chain. Residues of full-length furin that are not visible in the electron density or not in the crystallized protein are shown with a gray background.



better-diffracting but much smaller triclinic crystals, both containing eight molecules per asymmetric unit (**Table 1**). We have determined its molecular structure using MAD methods and phase extension by eight-fold cyclic noncrystallographic symmetry (NCS) averaging, and refined it at 2.6 Å resolution. In the final model, all eight furin chains are well defined in the electron density map from Tyr110 to Ala574, whereas for some molecules the first and last visible residues are Asp108 and Leu578, respectively. The polypeptide chain is folded into two separate but abutting domains, the spherical catalytic domain (Tyr110–Ala445) and the barrel-like P domain (Pro446–Thr573), which interact with each other through a tight 1,100 Å$^2$ interface.

## Catalytic domain

The core of the catalytic domain consists, similar to subtilisin[15,17], of a highly twisted β-sheet composed of seven parallel and one antiparallel β-strands (Cβ1–Cβ8, **Figs. 1** and **2**), flanked by five adjacent (Cα2–Cα6) and two peripheral helices (Cα1 and Cα7) and by two β-hairpin loops. However, a number of extended surface loops, several of them surrounding and shaping the active site cleft or mediating interaction with the P domain, show quite different lengths and conformations than those observed in bacterial subtilisins (**Fig. 3**). The catalytic domain of furin is cross-connected by disulfide bridges Cys211–Cys360 and Cys303–Cys333 (ref. 15) (**Fig. 3**). At two sites, it contains internally bound metal ions, which we identified as calcium ions on the basis of electron density, counter charges, oxygen coordination and distance criteria (**Figs. 2** and **3**). Calcium 1, enwrapped by loop segment Ala204–Gly212 similarly to subtilisin[15,17], is hepta-coordinated by three carbonyl oxygens and the carboxylate oxygens of Asp115, Asp162 (twice) and Asn208. Calcium 2, situated below the S1 pocket and coordinated by the carboxylate oxygens of Glu331 (twice), Asp258 and Asp301 and three internal solvent molecules, represents a previously unrecognized site in subtilases that was not predicted from modeling[15]. This calcium ion seems to stabilize the S1 pocket. However, furin does not contain the 'second' calcium site within the Asp177–Asp181 loop, which was anticipated as a result of the presumed homology to thermitase[15]. At a third site, identical to the suggested Ca401 binding site in subtilisin Carlsberg[17], a spherical electron density surrounded by Thr309 O, Ser311 O, Thr314 O and Oγ as well as one water molecule has been observed, which has been modeled as water but could be interpreted as an additional, partially occupied calcium ion. Of the three potential N-linked oligosaccharide sites, as many as 11 sugars are defined by electron density at Asn440, and one at Asn387 (**Fig. 2b**).

## P domain

The adjacent P domain is organized as a separate eight-stranded β-sandwich, as suggested from secondary structure predictions[16].

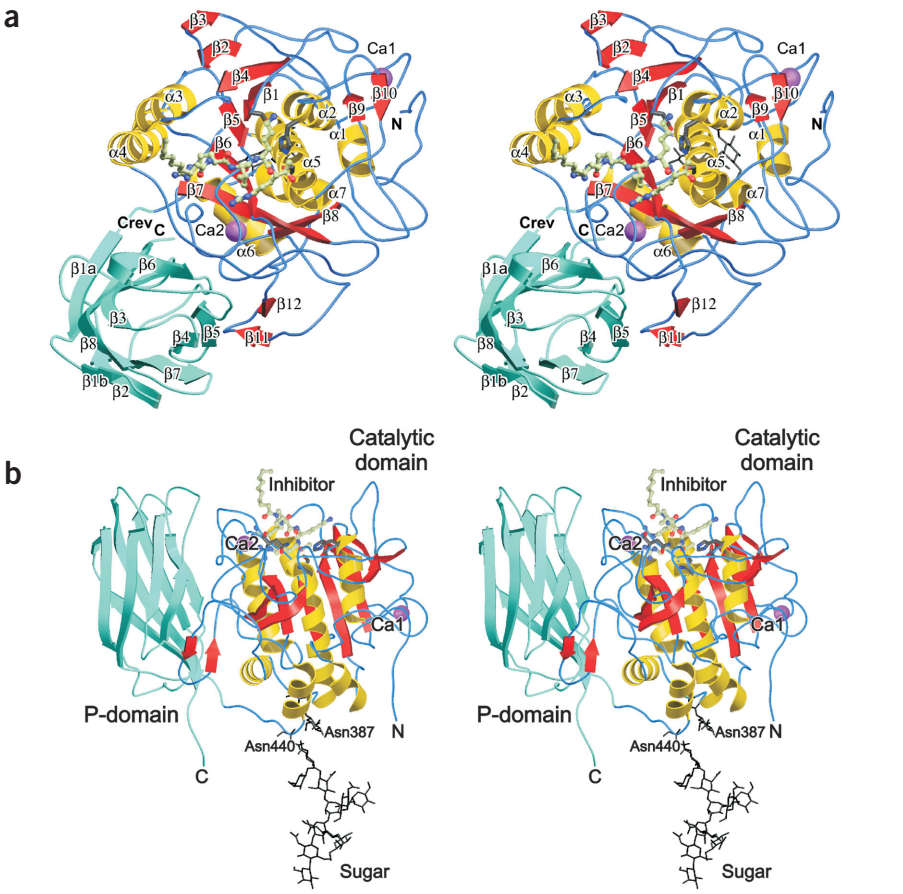


**Figure 2** Overall three-dimensional structure of mouse furin. (**a**) Stereo ribbon plot of soluble furin. Helices, β-strands and irregular structures of the catalytic domain are shown as yellow helices, red arrows and dark blue strands; the P domain is light blue. For clarity, the prefixes (C for catalytic and P for P domain) have been omitted from the secondary structure labels. The active site residues (dark gray) and the dec-RVKR-cmk inhibitor residues (light-colored ball-and-stick model) are given with all nonhydrogen atoms, and the two bound calcium ions as pink spheres. The deep crevice between the catalytic and the P domains (Crev) is of possible importance for propeptide, substrate binding or both. The view is toward the active-site cleft running horizontally across the catalytic domain surface. (**b**) Alternative orientation to **a**, showing more clearly the structurally defined N-linked oligosaccharides and the fold of the P domain. Full-length furin is anchored to the membrane by a probably flexible linker extending from the bottom of the P domain.

The strands are connected, however, as in jelly-roll β-barrels: that is, with β-strands Pβ1a/b-Pβ8-Pβ3-Pβ6 opposing β-strands Pβ2-Pβ7-Pβ4-Pβ5 (**Figs. 1** and **2**). The charged arginine and aspartic acid side chains of the Arg498-Gly-Asp segment, located at the Pβ3–Pβ4 loop, point in different directions and do not form a contiguous surface. This RGD structure is thus inconsistent with the suggested disintegrin or cellular routing function[18]. The closed structure of the P barrel suggests that only a complete P domain can fold stably and hence confer its stabilizing effect on the catalytic domain, in agreement with findings that in PC1/PC3 Thr594 (homologous to Thr573 located at the C-terminal end of the P domain of furin) is essential for activity[19]. According to secondary structure predictions, the rest of the chain down to the transmembrane domain should, except for a short helical segment, essentially consist of nonregular (coiled) structures (see **Fig. 1**). Hence, the ectodomain of membrane-anchored furin might be flexibly attached to the membrane, with the active site cleft preferentially pointing toward the lumen (**Fig. 2**).

The P domain 'edge' strands Pβ5 and Pβ6 and the large catalytic domain loops Cβ5–Cα4, Cβ6–Cβ7, Cβ7–Cβ8 and Cβ11–Cβ12 participate in interdomain contacts, mediated through a largely hydrophobic central patch[16] but also through a number of polar–salt bridge interactions. Therefore, the P domain presumably stabilizes the catalytic domain by shielding from solvent surface patches that are more hydrophobic than in subtilisin, and by interacting with several loops and segments of the catalytic domain that are substantially different in subtilisin and in furin (**Figs. 1** and **3**). These regions include the long Cβ11–Cβ12 hairpin loop as well as several residues forming the calcium 2 binding site, which stabilizes the S1 pocket (**Figs. 2** and **4**). The furin structure will allow for the rational design of subsequent experiments, to further explain the functional importance of the P domain.

In pro-furin, the presumably compact[14] but incompletely folded[20] propeptide, which acts as an intramolecular chaperone[9],

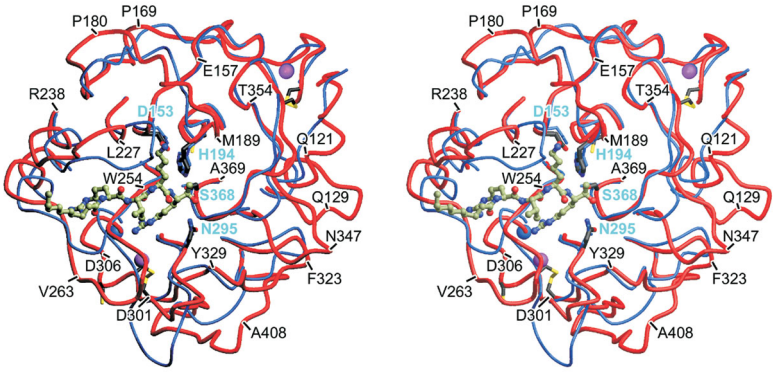


**Figure 3** Fold differences between subtilisin and the catalytic domain of furin. Superposition of a portion of the surface loops of the furin catalytic domain (red coil) with the equivalent loops in subtilisin Carlsberg[17] (blue coil), shown together with the bound dec-RVKR-cmk inhibitor (ball-and-stick model), the bound calcium ions of furin (pink sphere) and subtilisin (blue), as well as the two disulfide bonds of the catalytic domain of furin (orientation is as in **Fig. 1a**). Only a few residues central to the furin loops shown are labeled for orientation.

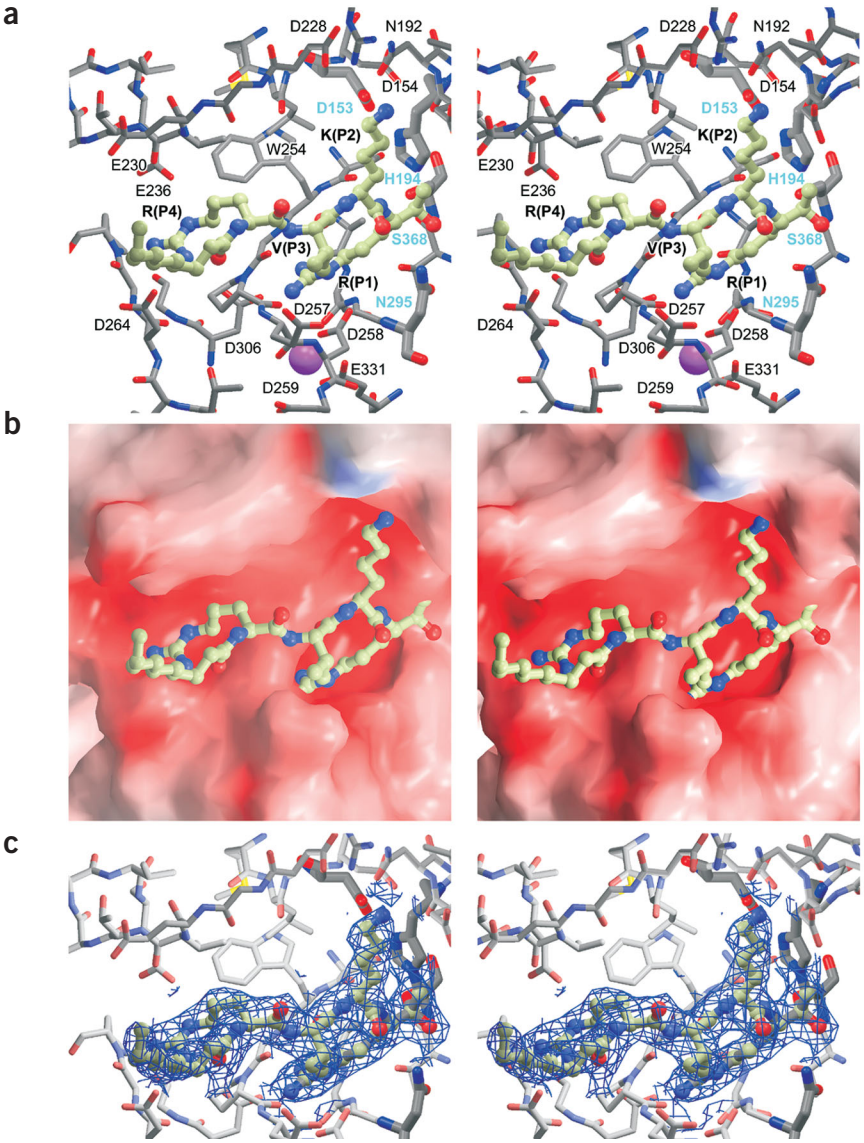


**Figure 4** Interactions between the inhibitor and the active site cleft. Stereo view toward the active site region of furin and the dec-RVKR-cmk inhibitor (orientation is similar to that in Fig. 1a). (**a**) Stick model of surrounding residues (dark gray carbons, blue nitrogens and red oxygens), shown together with the inhibitor (gray ball-and-stick model) and calcium 2 (purple sphere). The four inhibitor side chains, the active site residues and the acidic residues giving rise to negative electrostatic potential of subsites S1–S4 are labeled. (**b**) The inhibitor (ball-and-stick model) shown in front of the solid surface of the catalytic domain, colored according to its negative (red, $-27$ e $kT^{-1}$) and positive (blue, 27 e $kT^{-1}$) electrostatic surface potential. (**c**) Stick model similar to a, but with the dec-RVKR-cmk inhibitor superimposed with the final $2F_o - F_c$ electron density map (blue) contoured at 1σ.

might cap (similarly to the subtilisin BPN′–propeptide complex[21]) the N termini of helices Cα3 and Cα4, but in addition might bind into a furin-specific deep crevice formed between the catalytic and the P domain (**Figs. 2** and **5**). This positioning of the propeptide would allow the Arg-Ala-Lys-Arg107-↓-Asp108 cleavage segment (**Fig. 1**) to bind productively through the active site[21]. As discussed for the subtilisin–propeptide complex[21], such a productive alignment would require the partial unfolding of the next ten N-terminal residues (Asp108 to about Phe118) of the mature furin molecule, under concomitant disruption of calcium binding site 1.

### Active site cleft and inhibitor interaction

The active site cleft of furin differs considerably from that of bacterial subtilisins with respect to depth, shape and charges. In furin it is a canyon-like crevice, bounded by the exposed Cβ2–Cα2 loop and the Cβ4–Cα3 surface segment on one side and by the Cβ5–Cα4, Cβ6–Cβ7 and Cβ7–Cβ8 loops on the other side (**Figs. 2 and 4**), with the Ser368-His194-Asp153 active site triad arranged in its center. The P1-Arg carbonyl group of the bound dec-RVKR-cmk inhibitor, extending into the oxyanion hole formed by the carboxamide nitrogens of Asn295 and Ser368N, is covalently bound through Oγ and the methylene group of the tetrahedral hemiketal moiety (mimicking a transition state intermediate) with Ser368 and His194, respectively (with P1, P2 ... and P1′, P2′ ... designating substrate residues N- or C-terminal of the scissile peptide bond, opposing enzyme subsites S1, S2 … and S1′, S2′ …). The inhibitor's peptidyl moiety juxtaposes the extended Ser-Trp254-Gly-Pro-Glu257 segment, forming a twisted antiparallel β-sheet (**Fig. 4**). Unlike in subtilisin, segment Leu227–Thr232 is shorter and of different conformation in furin

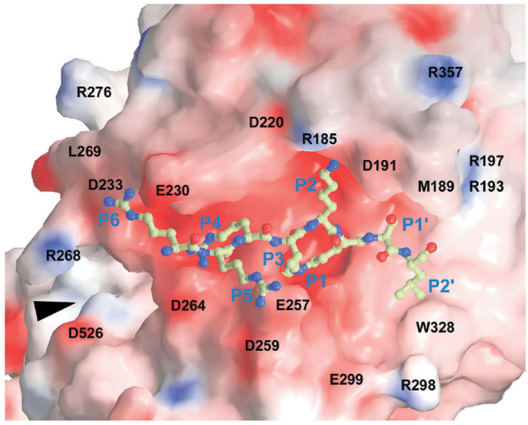


**Figure 5** A model of substrate interaction with furin. Solid surface representation of the extended active site cleft of mouse furin, shown together with an Arg-Arg-Arg-Val-Lys-Arg-↓-Ser-Leu substrate chain tentatively modeled into subsites from S6 to S2′ on the basis of the experimental inhibitor, eglin c[17] and the subtilisin–prodomain complex[21]. To the lower left, the entrance of the crevice formed between catalytic and P domain is indicated by an arrowhead. The surface has been colored according to the electrostatic surface potential of the catalytic domain. The orientation is as in the other figures.

**Table 1 Data collection and refinement statistics of the triclinic crystals**

**Data collection**

| Crystal | Native | Native | $Ta_6Br_{12}$ | | |
|---|---|---|---|---|---|
| | | | Edge | Peak | Remote |
| Detector | CCD | CCD + image plate | CCD | CCD | CCD |
| Space group | *P*1 | $P6_5$ | | $P6_5$ | |
| Unit cell dimensions | | | | | |
| *a* (Å) | 93.3 | 135.5 | | 135.8 | |
| *b* (Å) | 135.4 | 135.5 | | 135.8 | |
| *c* (Å) | 137.8 | 472.0 | | 472.7 | |
| α (°) | 103.6 | 90 | | 90 | |
| β (°) | 99.0 | 90 | | 90 | |
| γ (°) | 107.1 | 120 | | 120 | |
| Wavelength (Å) | 1.05 | 1.05 | 1.2552 | 1.25470 | 1.05 |
| Resolution (Å) | 18.83–2.60 | 36–2.70 | 34–3.95 | 34–3.95 | 34–3.95 |
| Number of reflections | | | | | |
| Measured | 382,695 | 874,780 | 328,928 | 324,973 | 334,120 |
| Unique | 182,735 | 133,288 | 85,626[a] | 84,871[a] | 86,054[a] |
| Completeness | | | | | |
| Overall | 97.7 | 99.7 | 99.4 | 98.6 | 99.7 |
| Outermost[b] | 97.2 (2.74–2.60) | 99.5 (2.75–2.70) | 98.7 (4.00–3.95) | 97.7 (4.00–3.95) | 97.7 (4.00–3.95) |
| $R_{sym}$ (%)[c] | | | | | |
| Overall | 10.0 | 11.4 | 7.6 | 7.9 | 7.5 |
| Outermost[b] | 34.7 (2.74–2.60) | 51.0 (2.75–2.70) | 11.0 (4.00–3.95) | 11.0 (4.00–3.95) | 9.6 (4.00–3.95) |

**Refinement statistics**

| | | | |
|---|---|---|---|
| Space group | *P*1 | Non-hydrogen atoms in the final model | |
| Resolution (Å) | 18.83–2.60 | protein + inhibitor | 28,991 |
| Number of reflections | | sugar atoms | 268 |
| Total | 182,726 | calcium | 16 |
| Test set | 9,564 | solvent | |
| Completeness (%)[d] | 97.9 (97.2) | water | 2,305 |
| *R*-factor (%)[d] | 18.8 (26.4) | sulfate | 350 |
| $R_{free}$ (%)[d,e] | 21.9 (31.0) | | |
| R.m.s. deviation from standard bond lengths (Å) | 0.007 | | |
| Average *B*-factor (Å$^2$)[f] | 21.3 (27.4) | | |
| *B*-factor r.m.s. deviation between bonded atoms (Å$^2$) | 1.402 | | |

[a]For the MAD data sets, Friedel pairs were counted as independent. [b]Values in parentheses show the last resolution shell in Å. [c]$R_{sym} = \Sigma_{hkl}\Sigma_i|I_{hkl,i} - \langle I\rangle_{hkl}| / \Sigma_{hkl,i}|\langle I\rangle_{hkl}|$. [d]Values for the last resolution shell (2.60–2.76 Å) are given in parentheses. [e]Calculated from 5.2% of the reflections, selected in thin shells and omitted from refinement. [f]Wilson plot *B*-factor in parentheses.

(**Fig. 3**) and does not, like the equivalent flexible 'lid' of subtilisin[17], add as a third outer strand to this short two-stranded β-sheet.

The P1-Arg side chain extends into the S1 pocket passing the curved Ser-Trp254-Gly-Pro-Asp257-Asp258 segment (often called 'entrance frame to the S1-pocket'; **Fig. 4a**), which is kinked more similarly to trypsin than to subtilisin (**Fig. 3**). This side chain is sandwiched between segments Ser253–Gly255 and Ser293–Asn295, with its guanidinium group perfectly packed between hydrophobic groups into a flat groove lined by the carboxylates of Asp258 and Asp306 and the carbonyls of Ala292 and Pro256. Any other side chain, including that of lysine, would fit less well, explaining the strict substrate requirement of furin for P1-Arg[1,5,22]. The P2-Lys side chain extends into a surface crevice, where its ε-ammonium group is surrounded by oxygens of the Asp154 carboxylate, the Asn192 carboxamide and the Asp191 carbonyl, for efficient hydrogen bonding (**Fig. 4**). Thus, the geometry and charge of this S2 subsite are beneficial for lysine accommodation but do not exclude a P2-Arg side chain. The P3-Val side chain extends into the bulk solvent, consistent with the lack of preference at this site (**Fig. 4**). However, side chains of alkaline P3 residues could make favorable contacts with the surface-located Glu257 carboxylate, favoring long basic P3 side chains, in agreement with the frequent presence of alkaline P3 residues in *in vivo* substrates of furin[5]. The kinked P4-Arg side chain extends into a cleft, where its guanidyl group is favorably framed by the carboxylate groups of Glu236 and Asp264 and packed against Trp254 and Tyr308 (**Figs. 4** and **5**). This complementary packing again favors accommodation of P4-Arg side chains, consistent with furin's strong preference for arginine and weaker preference for Lys-P4 residues[5], but permits occupation by other side chains.

### Extended substrate interaction

A comparison with the bound P6–P1 segment of the prodomain of the corresponding subtilisin BPN′ complex[21] suggests an extended conformation for P5–P6 residues (**Fig. 5**). Consequently, P5 side chains would run along the Cβ5–Cα4 loop across Glu257, whereas P6 side chains either should intercalate between the surface-located residues Glu230 and Asp233, or, in the case of short P4 residues, could thread into the S4 pocket opposite to P4 side chains (**Fig. 4a**). This idea is consistent with the observation that the majority of furin substrates possess alkaline residues at either P4 or P6 (refs. 1,5). The positively charged S1′ subsite seems to be designed preferentially to accommodate polar or negatively charged P1′ side chains, and S2′ for medium-sized hydrophobic residues (**Fig. 5**), in agreement with the required absence of lysine residues at P1′ and P2′ (refs. 1,5,19,23).

Thus, the targeting of substrates is dominated by extended electrostatic interactions through the 18 clustered negatively charged residues around the nonprime binding region of furin[15]. Whereas the S1, S2 and S4 subsites are specifically designed to accommodate arginine and lysine residues, the P3, P5 and P6 (even P7 and P8) residues mainly sense a negative surface potential, in accordance with furin's preference for polybasic peptide segments[24] (**Fig. 5**). Less positively charged peptide substrates might, as a result of insufficient charge compensation, be forced into a less optimal processing geometry, causing an incorrect presentation of the P1-P1′ peptide bond to the catalytic Ser368 Oγ. The polar charge distribution across the active site should help to preorient approaching peptide segments and to bring them into the correct register.

Sequence alignments suggest (data not shown) that the substrate binding clefts of the other PC members should be similar to furin, in agreement with the common reactivity toward dec-RVKR-cmk. However, all of the negatively charged subsites determined for furin can only be predicted for PC5/6. The other PCs should exhibit fewer negative charges at the S6 (PACE4, PC4) and additionally at the S3 and S5 subsites (PC2, PC1/PC3). These variations, and more subtle differences present in the direct environment of the distinct subsites, should allow for the development of specific inhibitors that are able to discriminate between the different PCs as required for targeted inhibition of distinct PCs in various scientific and potential therapeutic applications.

## DISCUSSION

The finding that lethal bacterial and viral pathogens require furin-mediated cleavage implies that strategies to target furin for therapeutic intervention could be fruitful[4]. Several protein-based inhibitor variants, such as the serpin α1-PDX, have been engineered to render them potent inhibitors of furin and the other PCs[1,4,5]. In addition, a number of synthetic furin inhibitors have been developed, most of which exhibit multibasic peptidyl moieties mimicking substrate or PC prodomain sequences[23,24], often linked to an active site–directed group such as chloromethylketone, ketomethylene or phosphonate[5,22,25]. Even in the light of various embryogenic and homeostatic functions of furin, specific, potent inhibitors might offer novel approaches especially for short-term antiviral and antibacterial therapy, by preventing maturation of pathogenic viruses and activation of bacterial toxins. This idea is supported by multiple studies indicating that furin inhibitors block cell death caused by *P. aeruginosa* and anthrax toxins as well as cytomegalovirus[4]. The lethal effect of *P. aeruginosa* toxin has also been blocked in mice by furin inhibitors[26]. The availability of an experimental furin structure will assist in the rational design of highly specific and potent inhibitors to target the activation of pathological substrates by furin.

## METHODS

**Crystallization.** The soluble ectodomain of mouse furin was expressed in dihydrofolate reductase (DHFR)–amplified CHO cells, and a C-terminally truncated, glycosylated ~60 kDa monomeric mature proteinase was purified from conditioned medium, as described[24]. SDS-PAGE, size exclusion chromatography, amino acid sequencing by Edman degradation and mass spectrometric analyses revealed that the final active proteinase starts with Asp108 and consists of 490 amino acid residues at maximum, probably extending as far as Pro582. This material was inhibited after purification with a four-fold molar excess of the dec-RVKR-cmk inhibitor. Triclinic and hexagonal crystals (**Table 1**) were obtained by mixing equal volumes of 10 mg $ml^{-1}$ protein solution and precipitant buffer (1.0 M $(NH_4)_2SO_4$, 0.4 M $Li_2SO_4$, 0.1 M sodium citrate, pH 6.0, with (hexagonal crystals) or without (triclinic crystals) 1,5-pentanediol) and equilibrating the mixture against the precipitant at room temperature.

**Data collection, model building and refinement.** Native X-ray data were collected directly (triclinic, to 2.6 Å resolution) or after transformation at 81% relative humidity[27] (hexagonal, to 2.7 Å resolution) from the shock-frozen crystals at 100 K at BW6/DORIS/Hamburg, using MarCCD and Mar345 image plate (IP) detectors (Mar-USA). In addition, derivative data were collected to 3.9 Å resolution from $Ta_6Br_{14}$-soaked transformed hexagonal crystals. Because of the large *c*-axis, the native hexagonal data set was merged from three IP measurements and one charge-coupled device (CCD) measurement. The data were processed and scaled using the HKL package[28] and MOSFLM/SCALA[29] (**Table 1**). Experimental 4.0 Å phases of high quality were obtained for the hexagonal crystals from a three-wavelength MAD experiment using nine $Ta_6Br_{12}^{2+}$ cluster sites, MLPHARE[29] and DM[29]. After phase extension to 2.7 Å by eight-fold cyclic density averaging and solvent flattening using DM[29] and manually determined initial averaging operators, a first furin model was built with MAIN[30] and partially refined with CNS version 1.1 (ref. 31). This model was used to determine with AmoRe[29] the orientation in the triclinic crystals. The triclinic structure was refined at 2.6 Å to an *R*-factor of 18.8 and an $R_{free}$ of 21.9% (**Table 1**), applying strong NCS restraints between the eight chains excluding a few short segments accounting for <10% of the residues. The test set for $R_{free}$ calculation was chosen in thin shells rather than at random to prevent correlation between the reflections in the test and refinement sets. Except for three residues (Asp158, Cys211 and Glu485) that are well defined in the electron density map and obviously exhibit high-energy conformations for all eight molecules, and one N-terminal Val109, which is weakly defined, all main chain angles fall into the most favored and additionally allowed regions of the Ramachandran plot[29]. Figures were prepared using GRASP[32], BobScript[33], MolScript[34], Raster3D[35] and ALSCRIPT[36].

**Coordinates.** The coordinates of furin have been deposited in the Protein Data Bank (accession code 1P8J).

ACKNOWLEDGMENTS

The technical help of H. Bartunik and R. Mentele and the financial support of a National Institutes of Health grant and a Research Scientist Development Award (I.L.), a DFG grant (M.E.T.), the SFB596, the Fonds der Chemischen Industrie and EU-projects (W.B.) are gratefully acknowledged. The authors wish to thank D. Steiner for establishing the contact for this collaboration.

COMPETING INTERESTS STATEMENT

The authors declare that they have no competing financial interests.

Received 23 April; accepted 20 May 2003
Published online 8 June 2003; doi:10.1038/nsb941

1. Nakayama, K. Furin: a mammalian subtilisin/Kex2p-like endoprotease involved in processing of a wide variety of precursor proteins. *Biochem. J.* **327**, 625–635 (1997).
2. Steiner, D.F. The proprotein convertases. *Curr. Opin. Chem. Biol.* **3**, 31–39 (1998).
3. Seidah, N.G. & Chretien, M. Proprotein and prohormone convertases: a family of subtilases generating diverse bioactive polypeptides. *Brain Res.* **848**, 45–62 (1999).
4. Thomas, G. Furin at the cutting edge: from protein traffic to embryogenesis and disease. *Nat. Rev. Mol. Cell Biol.* **3**, 753–766 (2002).
5. Rockwell, N.C., Krysan, D.J., Komiyama, T. & Fuller, R.S. Precursor processing by Kex2/furin proteases. *Chem. Rev.* **102**, 4525–4548 (2002).
6. Fuller, R.S., Brake, A.J. & Thorner, J. Intracellular targeting and structural conservation of a prohormone-processing endoprotease. *Science* 246, 482–486 (1989).

7. Siezen, R.J. & Leunissen, J.A. Subtilases: the superfamily of subtilisin-like serine proteases. *Protein Sci.* **6**, 501–523 (1997).
8. Anderson, E.D., VanSlyke, J.K., Thulin, C.D., Jean, F. & Thomas, G. Activation of the furin endoprotease is a multiple-step process: requirements for acidification and internal propeptide cleavage. *EMBO J.* 16, 1508–1518 (1997).
9. Anderson, E.D. *et al.* The ordered and compartment-specific autoproteolytic removal of the furin intramolecular chaperone is required for enzyme activation. *J. Biol. Chem.* 277, 12879–12890 (2002).
10. Roebroek, A.J. *et al.* Failure of ventral closure and axial rotation in embryos lacking the proprotein convertase Furin. *Development* **125**, 4863–4876 (1998).
11. Molloy, S.S., Bresnahan, P.A., Leppla, S.H., Klimpel, KR & Thomas, G. Human furin is a calcium-dependent serine endoprotease that recognizes the sequence Arg-X-X-Arg and efficiently cleaves anthrax toxin protective antigen. *J. Biol. Chem.* **267**, 16396–16402 (1992).
12. Volchkov, V.E., Feldmann, H., Volchkova, V.A. & Klenk, H.D. Processing of the Ebola virus glycoprotein by the proprotein convertase furin. *Proc. Natl. Acad. Sci. USA* **95**, 5762–5767 (1998).
13. Hallenberger, S. *et al.* Inhibition of furin-mediated cleavage activation of HIV-1 glycoprotein gp160. *Nature.* 360, 358–361 (1992).
14. Tangrea, M.A., Bryan, P.N., Sari, N. & Orban, J. Solution structure of the prohormone convertase 1 pro-domain from *Mus musculus*. *J. Mol. Biol.* **320**, 801–812 (2002).
15. Siezen, R.J., Creemers, J.W. & Van de Ven, W.J. Homology modelling of the catalytic domain of human furin. A model for the eukaryotic subtilisin-like proprotein convertases. *Eur. J. Biochem.* **222**, 255–266 (1994).
16. Ueda, K. *et al.* Mutational analysis of predicted interactions between the catalytic and P domains of prohormone convertase 3 (PC3/PC1). *Proc. Natl. Acad. Sci. USA* **100**, 5622–5627 (2003).
17. Bode, W., Papamokos, E. & Musil, D. The high-resolution X-ray crystal structure of the complex formed between subtilisin Carlsberg and eglin c, an elastase inhibitor from the leech *Hirudo medicinalis*. *Eur. J. Biochem.* **166**, 673–692 (1987).
18. Lusson, J. *et al.* The integrity of the RRGDL sequence of the proprotein convertase PC1 is critical for its zymogen and C-terminal processing and for its cellular trafficking. *Biochem. J.* **326**, 737–744 (1997).
19. Zhou, A., Martin, S., Lipkind, G., LaMendola, J. & Steiner, D.F. Regulatory roles of the P domain of the subtilisin-like prohormone convertases. *J. Biol. Chem.* **273**, 11107–11114 (1998).
20. Bhattacharjya, S. *et al.* pH-induced conformational transitions of a molten-globule-like state of the inhibitory prodomain of furin: implications for zymogen activation. *Protein Sci.* 10, 934–942 (2001).
21. Gallagher, T., Gilliland, G., Wang, L. & Bryan, P. The prosegment-subtilisin BPN' complex: crystal structure of a specific 'foldase'. *Structure* 3, 907–914 (1995).
22. Jean, F., Boudreault, A., Basak, A., Seidah, N.G. & Lazure, C. Fluorescent peptidyl substrates as an aid in studying the substrate specificity of human prohormone convertase PC1 and human furin and designing a potent irreversible inhibitor. *J. Biol. Chem.* **270**, 19225–19231 (1995).
23. Fugère, M. *et al.* Inhibitory potency and specificity of subtilase-like pro-protein convertase (SPC) prodomains. *J. Biol. Chem.* **277**, 7648–7656 (2002).
24. Cameron, A., Appel, J., Houghten, R.A. & Lindberg, I. Polyarginines are potent furin inhibitors. *J. Biol. Chem.* **275**, 36741–36749 (2000).
25. Basak, A., Zhong, M., Munzer, J.S., Chretien, M. & Seidah, N.G. Implication of the proprotein convertases furin, PC5 and PC7 in the cleavage of surface glycoproteins of Hong Kong, Ebola and respiratory syncytial viruses: a comparative analysis with fluorogenic peptides. *Biochem. J.* 353, 537–545 (2001).
26. Sarac, M.S., Cameron, A. & Lindberg, I. The furin inhibitor hexa-D-arginine blocks the activation of *Pseudomonas aeruginosa* exotoxin A *in vivo*. *Infect. Immun.* 70, 7136–7139 (2002).
27. Kiefersauer, R. *et al.* A novel free-mounting system for protein crystals: transformation and improvement of diffraction quality by accurately controlled humidity changes. *Appl. Crystallogr.* **33**, 1223–1230 (2000).
28. Otwinowski, Z. & Minor, W. Processing of X-ray diffraction data collected in oscillations mode. *Methods Enzymol.* **276**, 307–326 (1997).
29. Collaborative Computational Project, Number 4. The CCP4 Suite: Programs for Protein Crystallography. *Acta Crystallogr. D* 50, 760–763 (1994).
30. Turk, D. Weiterentwicklung eines Programms f_r Molekuelgraphik ]und Elektrondichte-Manipulation und seine Anwendung auf verschiedene Protein-Strukturaufklärungen. Dissertation, Technische Universität München (1992).
31. Brünger, A.T. *et al.* Crystallography and NMR system: a new software suite for macromolecular structure determination. *Acta Crystallogr. A* **54**, 905–921 (1998).
32. Nicholls, A., Bharadwaj, R. & Honig, B. Grasp: graphical representation and analysis of surface properties. *Biophys. J.* **64**, A166 (1993).
33. Esnouf, R.M. Further additions to MolScript version 1.4, including reading and contouring of electron density maps. *Acta Crystallogr. D* **55**, 938–940 (1999).
34. Kraulis, P. J. MolScript: a program to produce both detailed and schematic plots of protein structures. *J. Appl. Crystallogr.* **24**, 946–950 (1991).
35. Merritt, E.A. & Bacon, D.J. Raster3D: photorealistic molecular graphics. *Methods Enzymol.* **277**, 505–524 (1997).
36. Barton, G.J. ALSCRIPT: a tool to format multiple sequence alignments. *Protein Eng.* **6**, 37–40 (1993).

# A unique serine-specific elongation factor Tu found in nematode mitochondria

**Takashi Ohtsuki, Aya Sato, Yoh-ichi Watanabe & Kimitsuna Watanabe**
***Nat. Struct. Biol.* 9, 669–673 (2002).**

**Figure 3a** in this paper contained a mistake. In the tRNA sequence depicted in this panel, the $47^{th}$ and $48^{th}$ positions are C and U, respectively. We apologize for any inconvenience this may have caused.



# The crystal structure of the proprotein processing proteinase furin explains its stringent specificity

**Stefan Henrich, Angus Cameron, Gleb P Bourenkov, Reiner Kiefersauer, Robert Huber, Iris Lindberg, Wolfram Bode & Manuel E Than**
***Nat. Struct. Biol.* 10, 520–526 (2003).**

During the proofing stage of this paper, a publication presenting the crystal structure of Kex2, the homolog of furin in yeast, in complex with an inihibitor (Holyoak *et al. Biochemistry* **42**, 6709–6718; 2003) appeared online. We regret not having mentioned this work as a 'Note added in proof'. The full reference for Holyoak *et al.* is included here.

Holyoak, T. *et al.* 2.4 Å resolution crystal structure of the prototypical hormone-processing protease Kex2 in complex with an Ala-Lys-Arg boronic acid inhibitor. *Biochemistry* **42**, 6709–6718 (2003).